Coherent Acoustic Phonon Oscillations and Transient Critical Point Parameters of Ge from Femtosecond Pump–Probe Ellipsometry

Carola Emminger,* Shirly Espinoza, Steffen Richter, Mateusz Rebarz, Oliver Herrfurth, Martin Zahradník, Rüdiger Schmidt-Grund, Jakob Andreasson, and Stefan Zollner

Herein, the complex pseudodielectric function of Ge and Si from femtosecond pump–probe spectroscopic ellipsometry with 267, 400, and 800 nm pump–pulse wavelengths is analyzed by fitting analytical lineshapes to the second derivatives of the pseudodielectric function with respect to energy. This yields the critical point parameters (threshold energy, lifetime broadening, amplitude, and excitonic phase angle) of E_1 and $E_1 + \Delta_1$ in Ge and E_1 in Si as functions of delay time. Coherent longitudinal acoustic phonon oscillations with a period of about 11 ps are observed in the transient critical point parameters of Ge. From the amplitude of these oscillations, the laser-induced strain is found to be on the order of 0.03% for Ge measured with the 800 nm pump pulse, which is in reasonable agreement with the strain calculated from theory.

1. Introduction

In a recent publication,[1] the transient pseudodielectric function of Ge, Si, and InP obtained from femtosecond pump–probe spectroscopic ellipsometry (SE) between 1.7 and 3.5 eV using pump wavelengths of 267, 400, and 800 nm has been presented. Details on the experimental setup and the measurement results have been given in ref. [1] (the instrumental setup is also described

in ref. [2]); however, a quantitative analysis of the data has not been included. Therefore, the goal of this work is to quantitatively investigate the time-resolved critical points E_1 and $E_1 + \Delta_1$ in Ge and E_1 in Si using the data provided in ref. [1]. For this purpose, standard critical point lineshapes[3,4] are fitted to the second energy derivatives of the pseudodielectric function of both materials to obtain the critical point parameters (threshold energy, lifetime broadening, excitonic phase angle, and amplitude) as functions of delay time after optical excitation.

In the temporal evolution of the critical point parameters of Ge, oscillations are observed within the first 30 ps, which are identified as coherent longitudinal acoustic phonon (CAP) oscillations. The origin of such oscillations is a laser-induced hydrostatic strain pulse, which travels through the material.[5] CAP oscillations have been described in the literature[5–7] and have been measured in many different materials.[8–19] Although in general hard to detect in bulk semiconductors due to the large penetration depth,[9] CAP oscillations have been observed, for example, in the pump–probe reflectivity spectra of GaP and Si

C. Emminger, S. Zollner
Department of Physics
New Mexico State University
P.O. Box 30001 Las Cruces, NM 88003, USA

C. Emminger
Department of Condensed Matter Physics
Masaryk University
Kotlářská 267/2, 61137 Brno, Czech Republic

C. Emminger, O. Herrfurth, R. Schmidt-Grund
Felix-Bloch-Institut für Festkörperphysik
Universität Leipzig
Linnéstraße 5, 04103 Leipzig, Germany
E-mail: carola.emminger@uni-leipzig.de

C. Emminger
Institut für Physik
Humboldt-Universität zu Berlin
Zum Großen Windkanal 2, 12489 Berlin, Germany

S. Espinoza, S. Richter, M. Rebarz, M. Zahradník, J. Andreasson
ELI Beamlines
Fyzikální ústav AV ČR v.v.i.
Za Radnicí 835, 25241 Dolní Břežany, Czech Republic

S. Richter
Department of Physics
Faculty of Engineering (LTH)
Lund University
Box 118, 22100 Lund, Sweden

O. Herrfurth
Active Fiber Systems GmbH
Ernst-Ruska-Ring 17, 07745 Jena, Germany

R. Schmidt-Grund
Institut für Physik
Technische Universität Ilmenau
Weimarer Str. 32, 98693 Ilmenau, Germany

by Ishioka et al.,[9] in GaAs by Vinod et al.,[10] and Han et al.,[11] and in GaN by Wu et al.[12]

In the present study, it is shown that CAP oscillations can also be found in the transient critical point parameters of bulk Ge from femtosecond pump–probe SE measurements up to a delay time of about 30 ps. From the amplitude of the oscillations in the critical point energies, we are able to quantify the laser-induced strain using well-known deformation potentials and find it to be in reasonable agreement with the strain expected from theory. The analysis method is outlined in Section 2 and the results for Ge are discussed in Section 3, while the analysis results of Si are provided in Supporting Information.

2. Critical Point Analysis

The second derivatives of the pseudodielectric function with respect to energy are calculated by applying a linear filter method[20–23] using extended Gauss (EG) kernels,[24,25] which are defined as[21]

$$b_M(x) = \sum_{m=0}^{M} \left((-1)^m \frac{a^m}{m!} \frac{d^m}{da^m} \right) \frac{a^{-\frac{1}{2}}}{2\sqrt{\pi}} \exp\left(-\frac{x^2}{4a} \right) \quad (1)$$

where $\sqrt{a} = \Delta E$ is the width of the filter. Similar to the example given in Equation (21c) in ref. [21], one can define an expression using $b_4(x)$ and calculate the second derivatives with respect to energy. The pseudodielectric function is not given in equidistant energy or wavelength steps. Therefore, instead of converting from wavelength to energy, we calculate an average step size $\Delta E'_j = (E_{j+1} - E_{j-1})/2$ at each data point j. The second energy derivative of the data $\langle \varepsilon_i \rangle_j$, where $\langle \varepsilon_i \rangle$ can be either the real or imaginary part of the pseudodielectric function $\langle \varepsilon \rangle = \langle \varepsilon_1 \rangle + i \langle \varepsilon_2 \rangle$, is then given by

$$\frac{d^2 \langle \overline{\varepsilon}_i \rangle_{M=4}(E)}{dE^2} \approx \frac{1}{49152\sqrt{\pi}\Delta E^3} \sum_{j=j_1}^{j_2}$$
$$\times \left[\frac{E_{j+1} - E_{j-1}}{2} \langle \varepsilon_i \rangle_j \exp\left(-\frac{(E - E_j)^2}{4\Delta E^2} \right) \right.$$
$$\times \left(-110880 + \frac{188496(E - E_j)^2}{\Delta E^2} \right.$$
$$- \frac{45936(E - E_j)^4}{\Delta E^4} + \frac{3608(E - E_j)^6}{\Delta E^6}$$
$$\left. \left. - \frac{106(E - E_j)^8}{\Delta E^8} + \frac{(E - E_j)^{10}}{\Delta E^{10}} \right) \right] \quad (2)$$

For J data points, $j_1 = 2$ and $j_2 = J - 1$. The width ΔE of the filter is chosen according to the white noise onset of the Fourier coefficients obtained from a discrete Fourier transform, as explained in ref. [21,22]. To compute the Fourier transform and remove discontinuities at the endpoints of the data set, we use the method introduced in ref. [26]. The amount of noise in the data determines the white noise region and therefore the filter width (see, e.g., Figure 5 in ref. [21] or Section III in ref. [22]). In principle, one would have to determine the filter width for each data set separately. However, since the number of data

sets for each material and pump–pulse wavelength is >200, we determine ΔE at some selected delay times before, at, and after the pump pulse and choose the filter width that works best for all selected data sets. Table S1, Supporting Information, lists the chosen filter widths, the range of the step size, the spectral energy range, the energy range used for the fit, the time range (before and after the pump pulse), and the carrier concentration for both materials measured with various pump–pulse wavelengths.

We have ignored the depth dependence of the dielectric function (interference effects) and analyzed the pseudodielectric function of the sample. To fit the analytical lineshapes to the second energy derivatives of $\langle \varepsilon_1 \rangle$ and $\langle \varepsilon_2 \rangle$ using Equation (2), a Levenberg–Marquardt algorithm as explained in Chapter 15.5 in ref. [27] was implemented in C++. Starting parameters for the eight fit parameters (amplitude, energy, broadening, and phase angle for both E_1 and $E_1 + \Delta_1$, cf. Equations (3) and (4)) are taken based on steady-state values found in the literature.[28,29] At each delay time, all eight parameters are fitted to both $d^2 \langle \varepsilon_1 \rangle / dE^2$ and $d^2 \langle \varepsilon_2 \rangle / dE^2$, by minimizing the sum of the χ^2 merit functions of $d^2 \langle \varepsilon_1 \rangle / dE^2$ and $d^2 \langle \varepsilon_2 \rangle / dE^2$. The code automatically fits the data sets at all delay times using the same starting parameters for each case. **Figure 1** shows the second derivatives in the range of E_1 and $E_1 + \Delta_1$ in Ge measured with an 800 nm pump pulse, calculated from Equation (2) before ($t = -5$ ps), at ($t = 0$), and 3 ps after the pump pulse.
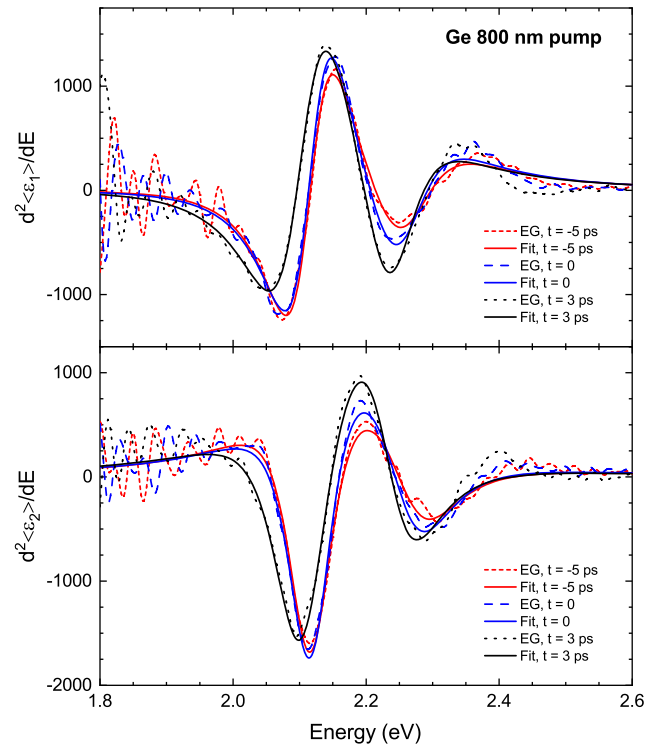

Figure 1. Second derivatives with respect to energy of the pseudodielectric function in the region of E_1 and $E_1 + \Delta_1$ of Ge measured with an 800 nm pump pulse (carrier concentration: 2×10^{20} cm^{-3}) at different delay times before (-5 ps), at ($t = 0$), and 3 ps after the pump pulse. Dashed lines represent the derivatives obtained as explained in the text. Solid lines represent the fits using 2D lineshapes for E_1 and $E_1 + \Delta_1$.

2200058 (2 of 7)

Solid lines show the fits with the second derivative of a 2D critical point lineshape, which best represents the E_1 and $E_1 + \Delta_1$ critical points,[29] given by

$$\frac{d^2\varepsilon(E)}{dE^2} = \frac{A_{E_1} e^{i\phi_{E_1}}}{(E - E_1 + i\Gamma_{E_1})^2} + \frac{A_{E_1+\Delta_1} e^{i\phi_{E_1+\Delta_1}}}{(E - (E_1 + \Delta_1) + i\Gamma_{E_1+\Delta_1})^2} \quad (3)$$

The fit parameters in Equation (3) are the amplitudes A_{E_1} and $A_{E_1+\Delta_1}$, the excitonic phase angles ϕ_{E_1} and $\phi_{E_1+\Delta_1}$, the critical point energies E_1 and $E_1 + \Delta_1$, and the broadenings Γ_{E_1} and $\Gamma_{E_1+\Delta_1}$. The agreement between the fit and the second derivatives calculated from the EG filters deteriorates between 2.3 and 2.5 eV. A possible explanation might be a structure that arises due to phase-filling effects[30] slightly above $E_1 + \Delta_1$. This has been simulated in ref. [30] for doped Ge with a carrier concentration of 10^{19} cm^{-3} at 77 K. Since the data we investigate in this work were measured at room temperature, we expect the structures shown in **Figure 2** of ref. [30] to feature a larger spectral broadening and therefore distort the lineshape of $E_1 + \Delta_1$. We suspect that this extra feature might be the reason of the deviations between the fits and the second derivatives above 2.3 eV in Figure 1, since the extra feature is not taken into account using the standard 2D critical point lineshape. In the case of Si, E_1 and $E_1 + \Delta_1$ cannot be distinguished since $\Delta_1 = 0.029$ eV is smaller than the E_1 broadening of about 0.1 eV at room temperature.[31] Therefore, we use a single 0D (excitonic) lineshape with the second derivative given by

$$\frac{d^2\varepsilon(E)}{dE^2} = \frac{-2A_{E_1} e^{i\phi_{E_1}}}{(E - E_1 + i\Gamma_{E_1})^3} \quad (4)$$

which best describes E_1 in Si according to Lautenschlager et al.[31]

3. Results and Discussion

3.1. Transient Critical Point Parameters of Ge

The measurements with a time resolution of 120 fs were performed on Ge(100) at an angle of incidence of 45° with respect to the surface normal for the *s*-polarized 35 fs pump pulses and 60° for the probe beam with the polarizer positions being fixed at ±45° (for further details on the experiment, see ref. [1]). Figure 2 depicts the critical point parameters as functions of delay time of Ge for pump–pulse wavelengths of 267, 400, and 800 nm obtained as explained in Section 2.

The vertical line marks the time $t = 0$ of the pump pulse. It should be noted that the delay time steps were not chosen to be constant. For Ge measured with the 800 nm pump pulse, for instance, the delay time steps were 10–50 fs between $t = -0.3$ and 1 ps, 100–250 fs between $t = 1$ and 10 ps, 1–2 ps between $t = 11$ to 30 ps, and 5–100 ps ($t > 30$ ps) (this is apparent in **Figure 3** and S1, Supporting Information, which depict the transient quantities as data points).

Several observations can be made about the critical point parameters of Ge. The E_1 and $E_1 + \Delta_1$ energies redshift after the pump pulse (except E_1 measured with a pump wavelength of $\lambda_{pump} = 400$ nm) and start to recover after about 4 ps. This
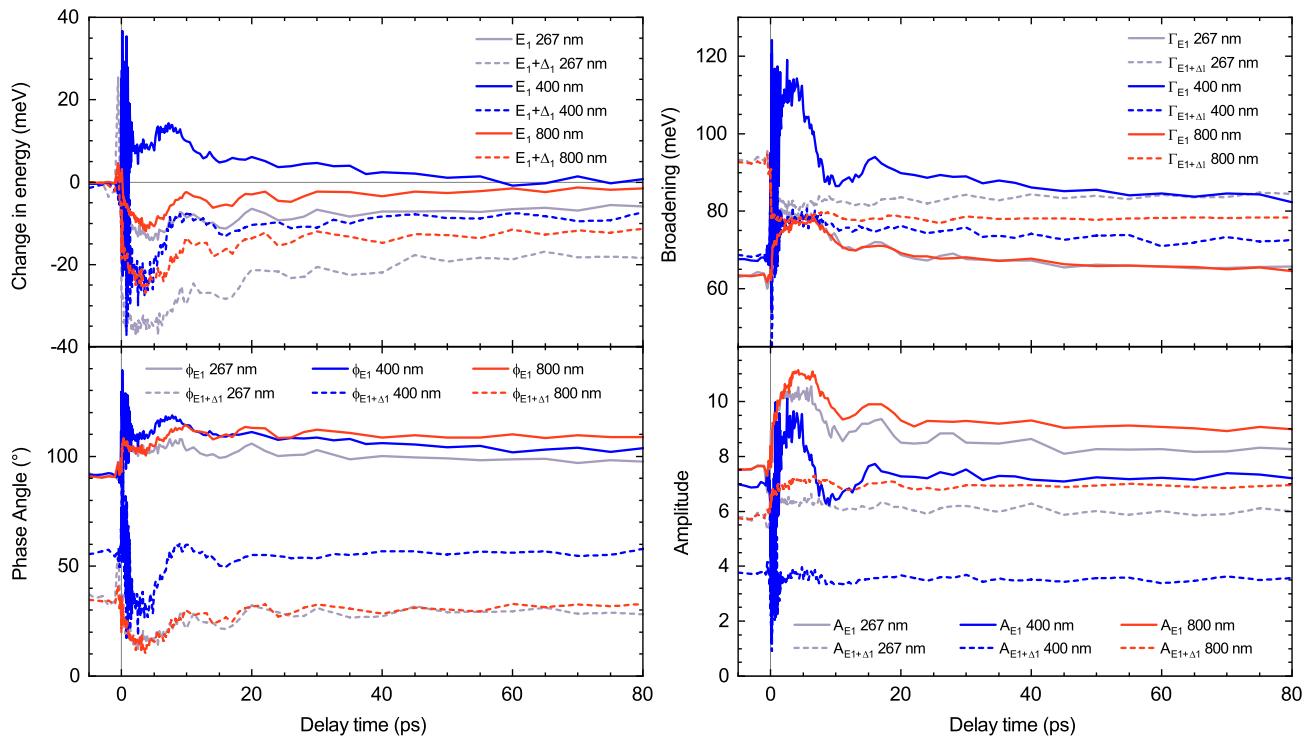

Figure 2. Temporal evolution of the critical point parameters of E_1 (solid) and $E_1 + \Delta_1$ (dashed) in bulk Ge (100) measured with pump–pulse wavelengths of 267 nm (gray), 400 nm (blue), and 800 nm (red).
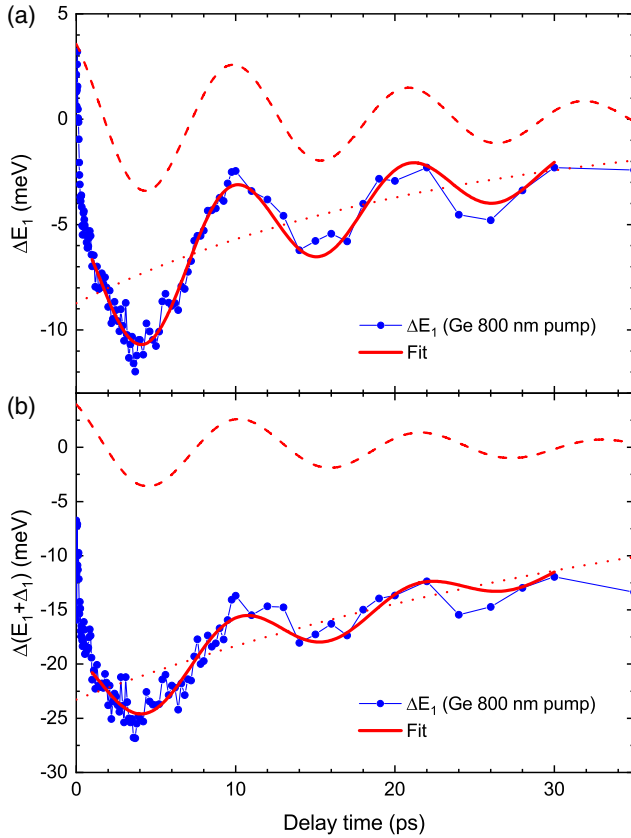
Figure 3. Spectral shifts ΔE_1 (change of the E_1 energies) and $\Delta(E_1 + \Delta_1)$ with delay time of Ge measured with the 800 nm pump pulse at a carrier concentration of 2×10^{20} cm^{-3}. The solid lines represent fits with Equation (7), which were performed between 1 and 30 ps. The oscillatory (first term in Equation (7)) and the decay term (second term in Equation (7)) are plotted using the fit parameters in Table 3 and are represented by the dashed and dotted lines, respectively.

redshift might be partially due to laser heating, although this does not explain why E_1 and $E_1 + \Delta_1$ do not shift by the same amount since Δ_1 is independent of temperature (the expected temperature increase is $\Delta T \approx 25$ K for the data measured with $\lambda_{\text{pump}} = 800$ nm,[1] which corresponds to a redshift of E_1 and $E_1 + \Delta_1$ of about 14 meV[28]). The data set measured with a pump wavelength of 400 nm shows an extraordinary feature at about 1.8 eV (this is possibly an experimental artifact, as discussed in Supporting Information of ref. [1]), which might affect the critical point parameters of E_1.

For $\lambda_{\text{pump}} = 267$ and 800 nm, the amplitudes of both E_1 and $E_1 + \Delta_1$ increase, while the pseudodielectric function shown in Figure 4 in ref. [1] and Figure S2, Supporting Information, suggests a decrease within the first couple of picoseconds. This is possibly related to the changes in the phase angles and broadenings of E_1 and $E_1 + \Delta_1$, which show opposite behavior for the two critical points: the broadening and phase angle of E_1 increase, while the parameters for $E_1 + \Delta_1$ decrease within the first couple of picoseconds after the pump pulse. Setting the phase angle equal for E_1 and $E_1 + \Delta_1$ as done in ref. [28] reduces the agreement between the fit and the calculated second derivatives.

Therefore, we treat both phase angles as fit parameters, which results in $\phi_{E_1} \approx 2\phi_{E_1 + \Delta_1}$. While the phase-filling effects might provide an explanation for the opposite behavior of the two critical points by affecting the lineshape of $E_1 + \Delta_1$ for the excited system (positive delay times), it should be noticed that some deviations of the critical point parameters were observed for the unpumped sample (i.e., at negative delay times). These discrepancies may originate from the treatment of the oxide layer, as discussed in ref. [2]. Interestingly, it seems that some parameters evolve with different rates and reach their final value faster than others (e.g., the $E_1 + \Delta_1$ amplitude measured with $\lambda_{\text{pump}} = 400$ nm). The origin of the different behavior of the two critical points is unclear at the present moment and will be addressed in a future publication including the analysis of newly measured data. In this study, we focus on the CAP oscillations whose amplitudes are on the same order of magnitude for both E_1 and $E_1 + \Delta_1$.

A discussion on the analysis results of the Si data is provided in Section 4 in Supporting Information.

3.2. Coherent Phonon Oscillations

Within the first 30 ps, CAP oscillations with a period of about 11 ps are observed in the critical point parameters of Ge, while no oscillations are detected for Si (possible explanations for the absence of CAP in the critical point parameters of Si are discussed later and in Supporting Information). The period of CAP oscillations is given by[7]

$$T = \frac{\lambda}{2n\nu_s \cos \theta} \tag{5}$$

where n is the (real part of the) refractive index of the material at the probe–beam wavelength λ, ν_s is the longitudinal sound velocity (given in **Table 1**), and θ is the angle of refraction.

Due to the large refractive index, the angle of refraction is small according to Snell's law and we can approximate

$$T \approx \frac{\lambda}{2n\nu_s} \tag{6}$$

Table 2 lists the probe wavelengths and corresponding refractive indices at E_1 and $E_1 + \Delta_1$ of Ge and E_1 of Si, as well as the period calculated from Equation (6) using values for the refractive index at the corresponding wavelengths from the literature.[32] Since we only intend to estimate the period, we do not consider

Table 1. Material parameters (as defined in the text) of Ge and Si at room temperature.

Parameter	Ge	Si	Ref.
B [N cm^{-2}]	7.5×10^6	9.8×10^6	[41]
β [K^{-1}]	5.9×10^{-6}	2.6×10^{-6}	[42,43]
C [J (cm$^3 \times$ K)$^{-1}$]	1.68	1.68	[44]
$\frac{\partial E_g}{\partial P}$ [eV Pa^{-1}]	5.0×10^{-11}	-1.5×10^{-11}	[40]
D_1^1 [eV]	-8.1		[45]
D_3^3 [eV]	5.9		[45]
ν_s [cm^{-1}]	4.91×10^5	9.36×10^5	[39,46]

ADVANCED SCIENCE NEWS
www.advancedsciencenews.com

pssrrl
physica status solidi
www.pss-rapid.com

Table 2. Wavelength λ and refractive index n at the E_1 and $E_1 + \Delta_1$ critical points of Ge and E_1 of Si, along with the period T of coherent longitudinal acoustic phonon oscillations calculated from Equation (6) and the penetration depth ζ.

	λ [nm]	n	T [ps]	ζ [nm]
E_1 in Ge	586.5[a]	5.68[b]	10.5	28
$E_1 + \Delta_1$ in Ge	536.7[a]	5.01[b]	10.9	18
E_1 in Si	365.3[c]	6.53[b]	3.0	11

[a]ref. [28] [b]ref. [32] [c]ref. [31]

the dependence on energy or delay time of the refractive index, which varies by about 2–3% within the first 10 ps.

The energy shifts shown in Figure 2 can be fitted with the sum of a damped oscillator (similar to ref. [9]) and an exponential decay.

$$\Delta E(t) = -\Delta E_a \cos\left(\frac{2\pi t}{T} - \delta\right) e^{-\frac{t}{\tau_a}} - \Delta E_b e^{-\frac{t}{\tau_b}} \tag{7}$$

Figure 3 shows the fit to the energy shifts ΔE_1 and $\Delta(E_1 + \Delta_1)$ with the fit parameters listed in **Table 3**, obtained from fitting the 800 nm pump–pulse data between 1 and 30 ps with Equation (7). Ishioka et al.[9] relate the buildup time of the strain pulse to the phase delay and therefore we treat the phase δ as a fit parameter as well. We performed the fits starting at 1 ps, that is, ignoring the strong decrease of the energies within the first picosecond, which is not (or not only) caused by the acoustic pulse.

The period of the oscillatory term of Equation (7), which is represented by the dashed lines in Figure 3, agrees very well with the calculated CAP periods given in Table 2. While $\Delta(E_1 + \Delta_1)$ is about twice as strong as ΔE_1, the amplitude ΔE_a of the oscillatory term is about the same for both critical points. Adding and subtracting the two amplitudes ΔE_a is used to estimate the strain inside the material due to the strain dependence of the E_1 and $E_1 + \Delta_1$ critical points via[33–35]

$$\Delta E_1 = \frac{\Delta_1}{2} + \Delta E_H - \sqrt{\frac{(\Delta_1)^2}{4} + (\Delta E_S)^2} \tag{8}$$

Table 3. Parameters obtained from fitting Equation (7) to the E_1 and $E_1 + \Delta_1$ shifts of Ge measured with the 800 nm pump pulse between 1 and 30 ps (Figure 3).

	$\Delta(E_1)$	$\Delta(E_1 + \Delta_1)$
ΔE_a [meV]	4.2 ± 0.3	4.6 ± 0.7
ΔE_b [meV]	8.7 ± 0.2	23.3 ± 0.5
T [ps]	11.0 ± 0.2	11.4 ± 0.4
δ [rad]	2.58 ± 0.06	2.6 ± 0.1
τ_a [ps]	20 ± 4	18 ± 7
τ_b [ps]	23 ± 2	42 ± 3

and

$$\Delta(E_1 + \Delta_1) = -\frac{\Delta_1}{2} + \Delta E_H + \sqrt{\frac{(\Delta_1)^2}{4} + (\Delta E_S)^2} \tag{9}$$

with the hydrostatic shift ΔE_H and the shear splitting ΔE_S given by[35]

$$\Delta E_H = \sqrt{3} D_1^1 \varepsilon_H \tag{10}$$

and

$$\Delta E_S = \sqrt{6} D_3^3 \varepsilon_S \tag{11}$$

where D_1^1 and D_3^3 are the shear and hydrostatic deformation potentials. The hydrostatic strain ε_H and shear strain ε_S depend on the in-plane ($\varepsilon_\parallel$) and out-of-plane ($\varepsilon_\perp$) strains in the following way[35]

$$\varepsilon_H = \frac{\varepsilon_\perp + 2\varepsilon_\parallel}{3} \tag{12}$$

$$\varepsilon_S = \frac{\varepsilon_\perp - \varepsilon_\parallel}{3} \tag{13}$$

We assume that the stress is isotropic (hydrostatic) and therefore set $\varepsilon_S = 0$ and $\varepsilon_{33} = \varepsilon_\perp = \varepsilon_\parallel$.[8,9] Adding Equations (8) and (9) and setting it equal to the sum of the two amplitudes, ΔE_a given in Table 3 results in $\Delta E_H = (4.4 \pm 0.4)$ meV. The hydrostatic strain can then be calculated using D_1^1 listed in Table 1, which gives $\varepsilon_H = (-3.1 \pm 0.3) \times 10^{-4}$. Similarly, subtracting Equation (9) from Equation (8) gives

$$\Delta_1 - 2\sqrt{\frac{(\Delta_1)^2}{4} + (\Delta E_S)^2} = -0.4\,\text{meV} \approx 0 \tag{14}$$

The amplitudes of the CAP oscillations are about the same for E_1 and $E_1 + \Delta_1$ considering the error bars, which is consistent with assuming $\Delta E_S = 0$.

To compare these results with the strain expected from theory, the expressions for the electron–hole and thermal contributions to the stress σ_{ij} given in Equation (17) and (18) in ref. [6] are used, which are

$$\sigma_{ij}^e = -B \frac{\partial E_g}{\partial P} \delta_{ij} N \tag{15}$$

and

$$\sigma_{ij}^p = -\frac{3B\beta}{C}(E - E_g)\delta_{ij} N \tag{16}$$

where B is the bulk modulus, $\partial E_g / \partial P$ is the pressure dependence of the indirect bandgap E_g, β is the linear thermal expansion coefficient, N is the number of photoexcited electron–hole pairs per unit volume, C is the specific heat, and E is the photon energy of the pump beam. The ratio of electronic and thermal contributions

ADVANCED SCIENCE NEWS
www.advancedsciencenews.com

pss rrl
physica status solidi
www.pss-rapid.com

Table 4. Ratio $\sigma_{ii}^e/\sigma_{ii}^p$ of the electron and thermal contributions to stress.

Pump wavelength	Ge	Si
800 nm	5.3	−7.5
400 nm	2.0	−1.6
267 nm	1.2	−0.9

$$\frac{\sigma_{ii}^e}{\sigma_{ii}^p} = \frac{C}{3\beta}\frac{\partial E_g}{\partial P}\frac{1}{(E-E_g)} \tag{17}$$

to the stress for different pump wavelengths is given in **Table 4**.

For the 800 nm pump pulse, the electron–hole contribution is much larger than the thermal contribution, while for the 267 nm pulse, the two contributions are about the same. The relation between the strain ε_{33} and stress tensor components is given by the compliance tensor components for diamond symmetry (O_h space group)[36,37]

$$\varepsilon_{33} = (S_{11} + 2S_{12})\sigma \tag{18}$$

where $\sigma = \sigma_{11} = \sigma_{22} = \sigma_{33}$ since the stress is isotropic.[8] The compliance tensor components can be calculated from $S_{11} + 2S_{12} = (C_{11} + 2C_{12})^{-1}$,[38] where the elastic constants C_{11} and C_{12} are components of the stiffness tensor. We use $C_{11} = 1.285 \times 10^7$ and $C_{12} = 0.483 \times 10^7\,\text{N cm}^{-2}$ for Ge (see Table 3.6a in ref. [38], which agrees with values provided by McSkimin[39]). For Ge measured with the 800 nm pump pulse, this results in

$$\varepsilon_{el} = (S_{11} + 2S_{12})\left(-B\frac{\partial E_g}{\partial P}N\right) \approx -6.4 \times 10^{-4} \tag{19}$$

and

$$\varepsilon_{ph} = (S_{11} + 2S_{12})\left(-\frac{3B\beta}{C}(E-E_g)\right) \approx -1.2 \times 10^{-4} \tag{20}$$

The total strain $\varepsilon_{33} = \varepsilon_{el} + \varepsilon_{ph} = -7.6 \times 10^{-4}$ compares reasonably well to the value of the out-of-plane strain estimated from the energy shift amplitudes ΔE_a. Using Equation (8) and (9), the calculated energy shifts are $\Delta E_1 = \Delta(E_1 + \Delta_1) = \Delta E_H = 11\,\text{meV}$, which is in reasonable agreement with ΔE_a of 4.3 and 4.5 meV in Table 3 considering the large uncertainty of the carrier concentration.

In the case of Si, the calculated strain ε_{33} is significantly smaller, on the order of 7×10^{-6} for the 267 and 800 nm pump–pulse data sets, and 2×10^{-5} for the data measured with the 400 nm pump pulse. Due to the negative pressure dependence of the indirect gap, which is $\partial E_g/\partial P = \partial E_{\Gamma X}/\partial P = -1.5 \times 10^{-11}\,\text{eV Pa}^{-1}$,[40] the electron–hole and thermal contributions do not add up as in the case of Ge, but partly cancel one another. A possible explanation for the non-detectability of CAP oscillations in the critical point parameters of Si (Figure S2, Supporting Information) might be the smaller wavelength of E_1 and the larger velocity of sound, which causes the strain pulse to leave the probed volume faster than for Ge, as illustrated in Figure S4, Supporting Information.

4. Conclusion

The pseudodielectric function of Ge and Si measured with pump–probe SE is analyzed by fitting analytical critical point line-shapes to the second derivatives of the pseudodielectric function with respect to energy to obtain energies, broadenings, excitonic phase angles, and amplitudes of the E_1 and $E_1 + \Delta_1$ critical points in Ge and E_1 in Si as functions of delay time. In the temporal evolution of E_1 and $E_1 + \Delta_1$ in Ge, CAP oscillations are observed. The measured period of 11 ps compares very well with the expected value. The pump–pulse-induced strain estimated from the amplitude of the oscillations in the energy shifts is in reasonable agreement with the strain calculated from theory. Coherent phonon oscillations are not detected in the case of Si, probably due to the shorter wavelength of E_1 and larger velocity of sound compared to Ge, which is related to the decay of the oscillations. Future work will address open questions regarding the behavior of the E_1 and $E_1 + \Delta_1$ critical point parameters by investigating effects related to the laser-induced carrier density by considering bandgap renormalization and phase-filling effects.

Supporting Information

Supporting Information is available from the Wiley Online Library or from the author.

Conflict of Interest

The authors declare no conflict of interest.

Data Availability Statement

The data that support the findings of this study are available in the Supporting Information of this article.

[1] S. Espinoza, S. Richter, M. Rebarz, O. Herrfurth, R. Schmidt-Grund, J. Andreasson, S. Zollner, *Appl. Phys. Lett.* **2019**, *115*, 052105.

[2] S. Richter, M. Rebarz, O. Herrfurth, S. Espinoza, R. Schmidt-Grund, J. Andreasson, *Rev. Sci. Instrum.* **2021**, *92*, 033104.

[3] M. Cardona, in *Modulation Spectroscopy* (Eds: F. Seitz, D. Turnbull, H. Ehrenreich), Academic, New York **1969**.

[4] D. E. Aspnes, in *Handbook on Semiconductors* (Ed: M. Balkanski), North-Holland, Amsterdam, **1980**.

[5] C. Thomsen, J. Strait, Z. Vardeny, H. J. Maris, J. Tauc, *Phys. Rev. Lett.* **1984**, *53*, 989.

[6] C. Thomsen, H. T. Grahn, H. J. Maris, J. Tauc, *Phys. Rev. B* **1986**, *34*, 4129.

[7] H. T. Grahn, H. J. Maris, J. Tauc, *IEEE J. Quantum Electron.* **1989**, *25*, 2562.

[8] O. B. Wright, B. Perrin, O. Matsuda, V. E. Gusev, *Phys. Rev. B* **2001**, *64*, 081202.

[9] K. Ishioka, A. Rustagi, U. Höfer, H. Petek, C. J. Stanton, *Phys. Rev. B* **2017**, *95*, 035205.

[10] M. Vinod, G. Raghavan, V. Sivasubramanian, *Sci. Rep.* **2018**, *8*, 17706.

[11] X. Han, M. Wang, W. Zhao, X. Xing, K. Wang, P. Lu, *Opt. Comm.* **2020**, *461*, 125257.

[12] S. Wu, P. Geiser, J. Jun, J. Karpinski, J.-R. Park, R. Sobolewski, *Appl. Phys. Lett.* **2006**, *88*, 041917.

[13] K. Ishioka, K. Brixius, A. Beyer, A. Rustagi, C. J. Stanton, W. Stolz, K. Volz, U. Höfer, H. Petek, *Appl. Phys. Lett.* **2016**, *108*, 051607.

[14] K. Ishioka, A. Beyer, W. Stolz, K. Volz, H. Petek, U. Höfer, C. J. Stanton, *J. Phys.: Condens. Matter* **2019**, *31*, 094003.

[15] Y.-K. Huang, G.-W. Chern, C.-K. Sun, Y. Smorchkova, S. Keller, U. Mishra, S. P. DenBaars, *Appl. Phys. Lett.* **2001**, *79*, 3361.

[16] C.-K. Sun, J.-C. Liang, C. J. Stanton, A. Abare, L. Coldren, S. P. DenBaars, *Appl. Phys. Lett.* **1999**, *75*, 1249.

[17] J. Wang, Y. Hashimoto, J. Kono, A. Oiwa, H. Munekata, H. Sanders, C. J. Stanton, *Phys. Rev. B* **2005**, *72*, 153311.

[18] R. Liu, C. S. Kim, G. D. Sanders, C. J. Stanton, J. S. Yahng, Y. D. Jho, K. J. Yee, E. Oh, D. S. Kim, *Phys. Rev. B* **2005**, *72*, 195335.

[19] P. Babilotte, P. Ruello, D. Mounier, T. Pezeril, G. Vaudel, M. Edely, J.-M. Breteau, V. Gusev, *Phys. Rev. B* **2010**, *81*, 245207.

[20] D. E. Aspnes, V. L. Le, Y. D. Kim, *J. Vac. Sci. Technol. B* **2019**, *37*, 051205.

[21] V. L. Le, T. J. Kim, Y. D. Kim, D. E. Aspnes, *J. Vac. Sci. Technol. B* **2019**, *37*, 052903.

[22] V. L. Le, T. J. Kim, Y. D. Kim, D. E. Aspnes, *J. Kor. Sci. Phys. Soc.* **2020**, *77*, 819.

[23] V. L. Le, Y. D. Kim, D. E. Aspnes, *Opt. Express* **2020**, *28*, 38917.

[24] D. K. Hoffman, T. L. Marchioro, M. Arnold, Y. Huang, W. Zhu, D. J. Kouri, *J. Math. Chem.* **1996**, *20*, 117.

[25] D. K. Hoffman, D. J. Kouri, E. Pollak, *Comput. Phys. Commun.* **2002**, *147*, 759.

[26] S. D. Yoo, D. E. Aspnes, *J. Appl. Phys.* **2001**, *89*, 8183.

[27] S. A. Teukolsky, B. P. Flannery, W. H. Press, W. T. Vetterling, *Numerical Recipes In C*, Press Syndicate of the University of Cambridge, New York, **1992**.

[28] N. S. Fernando, T. N. Nunley, A. Ghosh, C. M. Nelson, J. A. Cooke, A. A. Medina, S. Zollner, C. Xu, J. Menendez, J. Kouvetakis, *Appl. Surf. Sci.* **2017**, *421*, 905.

[29] L. Viña, S. Logothetidis, M. Cardona, *Phys. Rev. B* **1984**, *30*, 1979.

[30] C. Xu, N. S. Fernando, S. Zollner, J. Kouvetakis, J. Menéndez, *Phys. Rev. B* **2017**, *118*, 267402.

[31] P. Lautenschlager, M. Garriga, L. Viña, M. Cardona, *Phys. Rev. B* **1987**, *36*, 4821.

[32] D. E. Aspnes, A. A. Studna, *Phys. Rev. B* **1983**, *27*, 985.

[33] F. H. Pollak, *Surf. Sci* **1973**, *37*, 863.

[34] F. H. Pollak, M. Cardona, *Phys. Rev.* **1968**, *172*, 816.

[35] S. Zollner, in *Silicon-Germanium Carbon Alloys: Growth, Properties Applications* (Eds: S.T. Pantelides, S. Zollner), Taylor&Francis, New York **2002**, p. 387.

[36] J. F. Nye, *Physical Properties of Crystals*, Oxford University Press, Oxford **1969**.

[37] R. C. Powell, *Symmetry, Group Theory, The Physical Properties of Crystals*, Springer, New York **2010**.

[38] P. Y. Yu, M. Cardona, *Fundamentals of Semiconductors: Physics Materials Properties*, Springer, Heidelberg **1996**.

[39] H. J. McSkimin, P. Andreatch, *J. Appl. Phys.* **1964**, *35*, 3312.

[40] W. Paul, *J. Appl. Phys.* **1961**, *32*, 2082.

[41] L. E. Vorobyev, in *Handbook Series on Semiconductor Parameters, Vol. 1: Si, Ge, C (Diamond) GaAs, GaP, GaSb, InAs, InP, InSb* (Eds: M. Levinshtein, S. Rumyantsev, M. Shur), World Scientific, Singapore **1996**.

[42] G. A. Slack, S. F. Bartram, *J. Appl. Phys.* **1975**, *46*, 89.

[43] Y. Okada, Y. Tokumaru, *J. Appl. Phys.* **1984**, *56*, 314.

[44] D. Gerlich, B. Abeles, R. E. Miller, *J. Appl. Phys.* **1965**, *36*, 76.

[45] M. Chandrasekhar, F. H. Pollak, *Phys. Rev. B* **1977**, *15*, 2127.

[46] H. J. McSkimin, P. Andreatch, *J. Appl. Phys.* **1963**, *34*, 651.